Role of long-range interaction on the electrical transport and electron-phonon scattering in thermoelectric Mg_2Si

Chengliang Xia[1] and Yue Chen[1, 2, a)]

[1)] *Department of Mechanical Engineering, The University of Hong Kong, Pokfulam Road, Hong Kong SAR, China*

[2)] *HKU Zhejiang Institute of Research and Innovation, 1623 Dayuan Road, Lin An 311305, China*

(Dated: 1 March 2022)

Many thermoelectrics are polar materials where the long-range interaction plays a non-negligible role; however, its effect on the electrical transport property of thermoelectric materials is yet to be fully investigated. In this work, we demonstrate the importance of long-range interaction on the electrical transport property and the electron-phonon scattering mechanism in thermoelectric Mg_2Si. We find that the agreement between experimental and theoretical electrical conductivities can be significantly improved after considering long-range interaction. In addition, we also demonstrate the importance of long-range interaction for studying the effect of band convergence on thermoelectric properties.

[a)] Correspondence to yuechen@hku.hk.

Electron-phonon interaction has attracted much research attention in the thermoelectric field in recent years[1–5]. Explicit electron-phonon calculation is critical for evaluating the electronic relaxation time, which dominates the electronic scattering process in thermoelectric materials[6,7]. Electronic relaxation time is needed to calculate electrical conductivity and carrier mobility. Furthermore, electron-phonon interaction provides an in-depth understanding of the electronic scattering mechanism[8,9]. Most existing Wannier-interpolated electron-phonon calculations only consider the contribution from the short-range interaction, suitable for estimating the electrical transport property of non-polar semiconductors[10–13]. With the computational method of Fröhlich electron-phonon vertex proposed by Verdi and Giustino[14], the contribution of long-range interaction on the electron-phonon interaction can be studied[15–20]. Many thermoelectrics are polar materials where the long-range interaction plays a critical role[21–24]; however, the effect of long-range interaction on the electrical transport property of thermoelectric materials is yet to be fully investigated.

Band engineering is shown to be an effective method to improve the electrical transport performance of thermoelectric materials[25–31]. For example, by adjusting the doping composition, the valence band maxima of PbTe converge at the L point and along the Σ path of the Brillouin zone, leading to high Seebeck coefficient and electrical conductivity[25]. The lattice parameter ratio ($c/2a$) is crucial for controlling the band convergence in the tetragonal chalcopyrite compounds, such as $Cu_2FeGeSe_4$ and $Cu_2ZnGeSe_4$[32,33]. In these compounds, multiple valence bands converge at Γ point at critical lattice parameter ratios, resulting in increased power factors. Recently, Park et al. reported through their first-principles calculation of the $CaMg_2Sb_2$-$CaZn_2Sb_2$ Zintl system that if electronic bands converge at one k point, the band convergence is not beneficial for improving the electrical transport property[34]. They showed that the electrical conductivity and carrier mobility of a hypothetical light-band-only system are much larger than those of the fully converged system, leading to a larger peak power factor in the hypothetical light-band-only system.

In this work, we perform first-principles calculations to study the electrical transport and electron-phonon interaction of Mg_2Si. Under uniform triaxial tensile strains, different band structure configurations near the conduction band edge of Mg_2Si are achieved, and the corresponding electrical transport properties are studied. We compare the electrical conductivity, carrier mobility, and electronic scattering rate to demonstrate the importance of long-range interaction for thermoelectric Mg_2Si.

Density functional theory (DFT)[35,36] calculations were performed using Quantum Espresso[37,38]. Norm-conserving relativistic pseudopotential in the form of PBE parametrization[39,40] was applied with a kinetic energy cutoff of 80 Ry. A 10×10×10 k-mesh and a 5×5×5 q-mesh were used in the self-consistent and phonon calculations, respectively. The unit cells of unstrained and strained Mg_2Si were relaxed until the total energy converged to 10^{-7} Ry and the atomic forces smaller than 1×10^{-6} Ry/a.u.

The electronic self-energy that originates from the electron-phonon interaction was calculated using Electron-Phonon Wannier (EPW)[11,41].

$$\Sigma_{n\mathbf{k}}(\omega,T)=\frac{1}{\hbar}\sum_{mv}\int_{BZ}\frac{d\mathbf{q}}{\Omega_{BZ}}|g_{mn,v}(\mathbf{k},\mathbf{q})|^2\times[\frac{1-f_{m\mathbf{k+q}}(T)+n_{\mathbf{q}v}(T)}{\omega-\varepsilon_{m\mathbf{k+q}}+\varepsilon_F-\omega_{\mathbf{q}v}+i\delta} +\frac{f_{m\mathbf{k+q}}(T)+n_{\mathbf{q}v}(T)}{\omega-\varepsilon_{m\mathbf{k+q}}+\varepsilon_F+\omega_{\mathbf{q}v}+i\delta}] \quad (1)$$

where $g_{mn,v}(\mathbf{k},\mathbf{q})$ is electron-phonon matrix element, $f_{n\mathbf{k}}$ is Fermi-Dirac distribution, and $n_{\mathbf{q}v}$ is Bose-Einstein distribution. The imaginary part of the electronic self-energy corresponds to the electronic scattering rate, which is the inverse of the electronic relaxation time.

$$\frac{1}{\tau_{n\mathbf{k}}}=\frac{2\pi}{\hbar}\sum_{mv}\int\frac{d\mathbf{q}}{\Omega_{BZ}}|g_{mn,v}(\mathbf{k},\mathbf{q})|^2\times[(1-f_{m\mathbf{k+q}}+n_{\mathbf{q}v})\delta(\varepsilon_{n\mathbf{k}}-\hbar\omega_{\mathbf{q}v}-\varepsilon_{m\mathbf{k+q}}) +(f_{m\mathbf{k+q}}+n_{\mathbf{q}v})\delta(\varepsilon_{n\mathbf{k}}+\hbar\omega_{\mathbf{q}v}-\varepsilon_{m\mathbf{k+q}})] \quad (2)$$

Electron-phonon matrix elements were calculated with or without considering long-range interaction. The 10×10×10 k-mesh and the 5×5×5 q-mesh were interpolated to a 100×100×100 fine k-mesh and a 60×60×60 fine q-mesh, respectively, for the electron-phonon coupling calculation. Different k-meshes and q-meshes were tested, as shown in Figs. S1 and S2 in the Supporting Information. Using the electronic scattering rates, the calculations of the electrical transport property were performed based on the Boltzmann transport theory as implemented in BoltzTraP2[42].

First, we study the effect of long-range interaction on the electrical transport property of Mg_2Si, as shown in Fig. 1. Panels **a** and **b** depict the electrical conductivity of Mg_2Si at 300 K calculated without and with long-range interaction. Electrical conductivity calculated with long-range interaction is significantly lower than that calculated without long-range interaction. At electron carrier concentrations of 1×10^{20} cm^{-3} and 2×10^{20} cm^{-3}, the electrical conductivity of Mg_2Si calculated with long-range interaction is reduced by about 64.7% and 57.1%, respectively, compared with those calculated without considering long-range interaction.

The experimental electrical conductivities of Mg_2Si alloys are also shown in panels **a** and **b** for comparison. If only the short-range interaction is considered, the theoretical electrical conductivity of Mg_2Si is about 3-4 times larger than the experimental value. Similar differences between theoretical and experimental electrical conductivities were also observed in other thermoelectric materials in previous studies, such as GeTe[47] and Mg_3Sb_2[48]. Due to the overestimated theoretical electrical conductivity, the calculated power factor can be much larger than the experimental value, which limits a quantitative theoretical analysis of

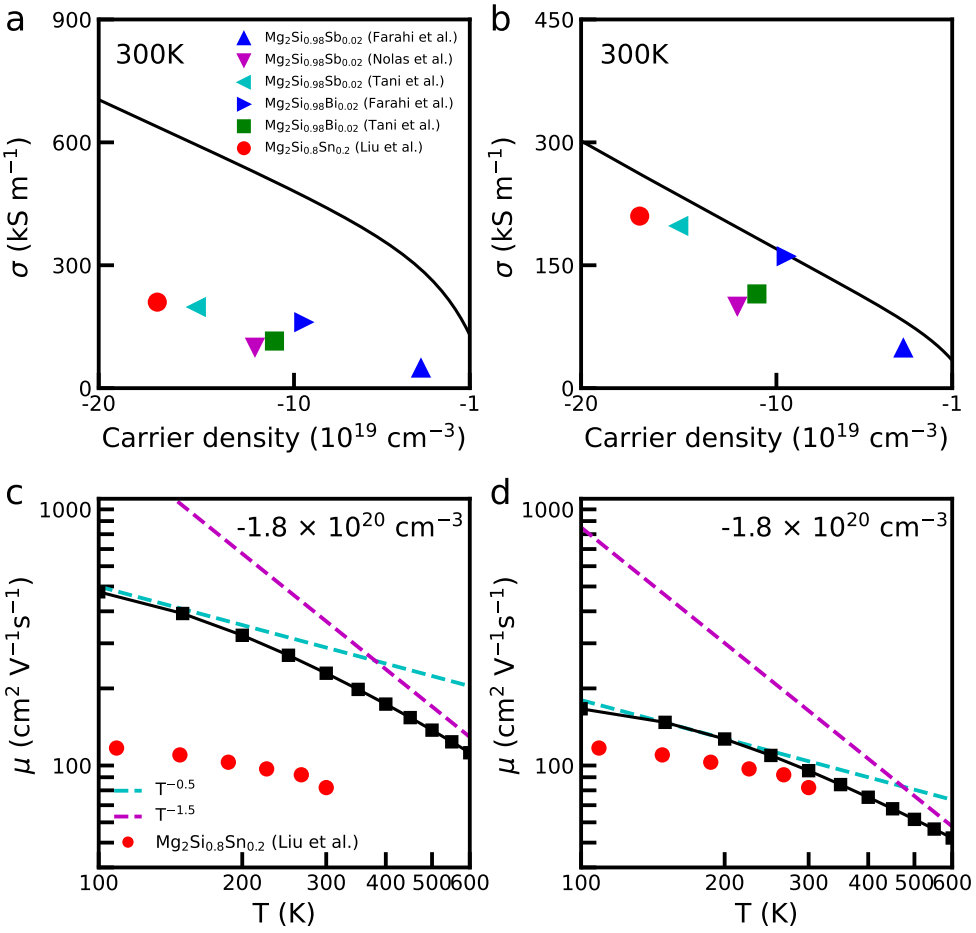

FIG. 1. Electrical conductivity of Mg_2Si at 300 K calculated without (**a**) and with (**b**) long-range interaction. Experimental electrical conductivities[14,43–46] are also included in panels **a** and **b** for comparison. Electron carrier densities are denoted by negative values. Carrier mobility of Mg_2Si (at -1.8 × 10^{20} cm^{-3}) under different temperatures calculated without (**c**) and with (**d**) long-range interaction. Experimental carrier mobility of $Mg_2Si_{0.8}Sn_{0.2}$[14] is also shown in panels **c** and **d** for comparison.

the electrical transport property of thermoelectric materials. It is seen from Fig. 1**b** that after the long-range interaction is considered, the theoretical electrical conductivity reduces significantly and becomes much closer to the experimental data.

Carrier mobilities of Mg_2Si under different temperatures calculated without and with long-range interaction are shown in Fig. 1**c** and **d**, respectively. These carrier mobilities correspond to an electron carrier concentration of 1.8×10^{20} cm^{-3}, facilitating a direct comparison with the experimental data of $Mg_2Si_{0.8}Sn_{0.2}$. In a temperature range from 100 K to 600 K, the carrier mobility of Mg_2Si calculated with long-range interaction is smaller than that calculated without long-range interaction. By considering long-range interaction, our theoretical results agree better with the experimental mobility of $Mg_2Si_{0.8}Sn_{0.2}$. The larger theoretical carrier mobilities of Mg_2Si than the experimental values can be related to the fact that only the electronic scattering by phonons is considered in our calculation. Kutorasiński et al. found that impurity scattering can account for about a 6% reduction of the total electrical conductivity of Mg_2Si-based alloys[49]. Furthermore, it was found from experiments that the temperature dependence of the carrier mobility of $Mg_2Si_{1-x}Sn_x$ near 300 K is approximately $\mu \propto T^{-0.5}$. With long-range interaction, we see from Fig. 1**d** that the temperature dependence of the theoretical carrier mobility of Mg_2Si is closer to $\mu \propto T^{-0.5}$ near room temperature. Overall, the long-range interaction can significantly amend the calculated electrical conductivity and carrier mobility, and thus it plays a vital role in the quantitative analysis of the electrical transport properties of thermoelectric materials.

The effects of long-range interaction on the electrical transport property and electron-phonon scattering mechanism of Mg_2Si under strains are further studied. Uniform triaxial tensile strain is an effective method to control band structure configurations and to achieve band convergence in Mg_2Si[50]. Fig. 2 shows the band structures of Mg_2Si under different uniform triaxial tensile strains. Blue and green lines represent the lowest and the second-lowest conduction bands in unstrained Mg_2Si, respectively. The conduction band minimum (CBM) of unstrained Mg_2Si locates at X point, and the energy offset of the minima of the two lowest conduction bands at X point is 0.19 eV. This energy offset gradually decreases when tensile strain increases. These two lowest conduction bands converge under a 2.4% tensile strain. With further increasing tensile strain, the blue conduction band edge increases continuously, and the green band becomes the lowest conduction band. The energy offset at X point thus becomes -0.11 eV under a 4% tensile strain. The phonon dispersion of strained

Mg_2Si does not exhibit any imaginary frequency, as shown in Fig. S3 in the Supporting Information, which indicates that Mg_2Si is dynamically stable even under a 4% tensile strain.

Panels **a** and **b** of Fig. 3 compare the electrical conductivity of Mg_2Si at 300 K under different uniform triaxial tensile strains calculated without and with long-range interaction. It is noticed from Fig. 3**a** that the electrical conductivity of Mg_2Si under a 4% tensile strain is larger than that under a 2.4% tensile strain in a wide range of carrier concentrations. However, when the long-range interaction is taken into account, the electrical conductivities of Mg_2Si under different tensile strains are all suppressed, and the largest electrical conductivity of Mg_2Si is observed at a 2.4% tensile strain, where the conduction bands converge

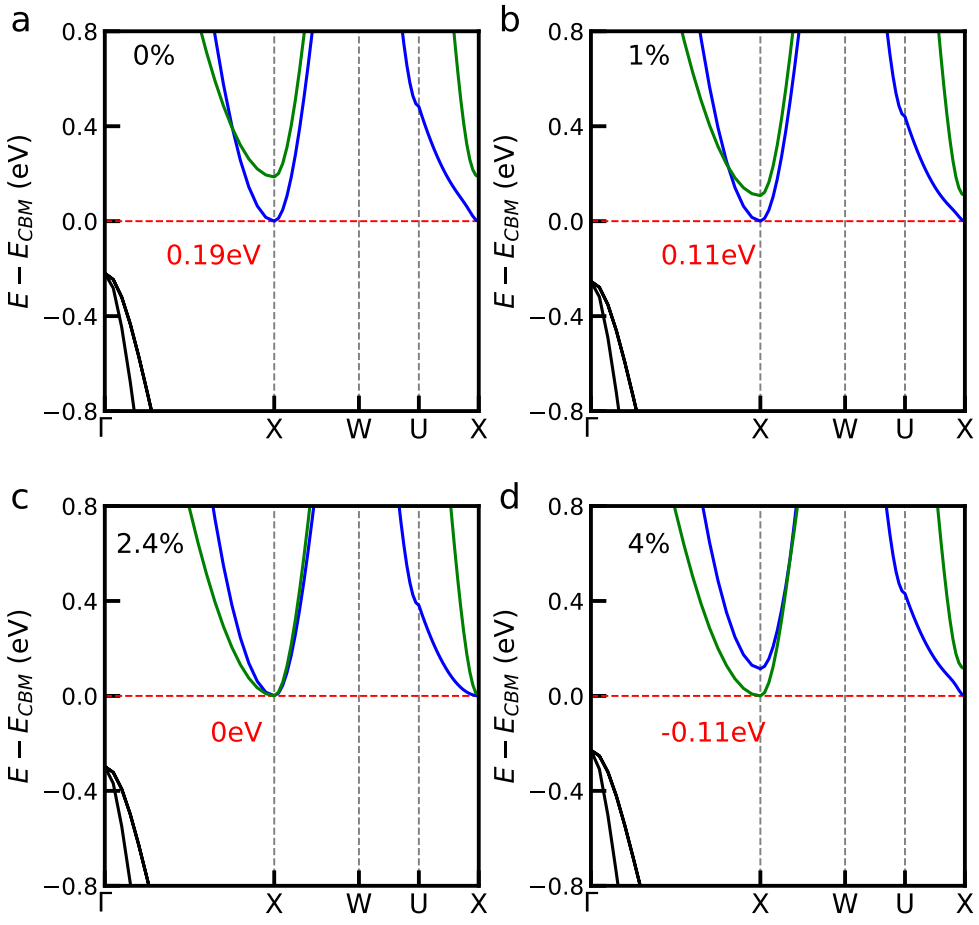

FIG. 2. Band structures of Mg_2Si under uniform triaxial tensile strains. Tensile strain value and the energy offset of the minima of the two lowest conduction bands at X point are given in each panel. The conduction band minimum (CBM) is shifted to 0 eV.

at X point. In addition, we also show the Seebeck coefficient and power factor of Mg_2Si under different tensile strains in Fig. S4 of the Supporting Information. The Seebeck coefficient of Mg_2Si under a 2.4% tensile strain is much larger than that under other tensile strains, thus the power factor is the largest under a 2.4% tensile strain, regardless whether the long-range interaction is considered or not. The band convergence strategy is beneficial to improving the electrical transport property of Mg_2Si where the significant increase of Seebeck coefficient dominates the change of power factor.

Panels **c** and **d** of Fig. 3 show the carrier mobility of Mg_2Si under different uniform triaxial tensile strains from 100 K to 600 K without and with long-range interaction, respectively.

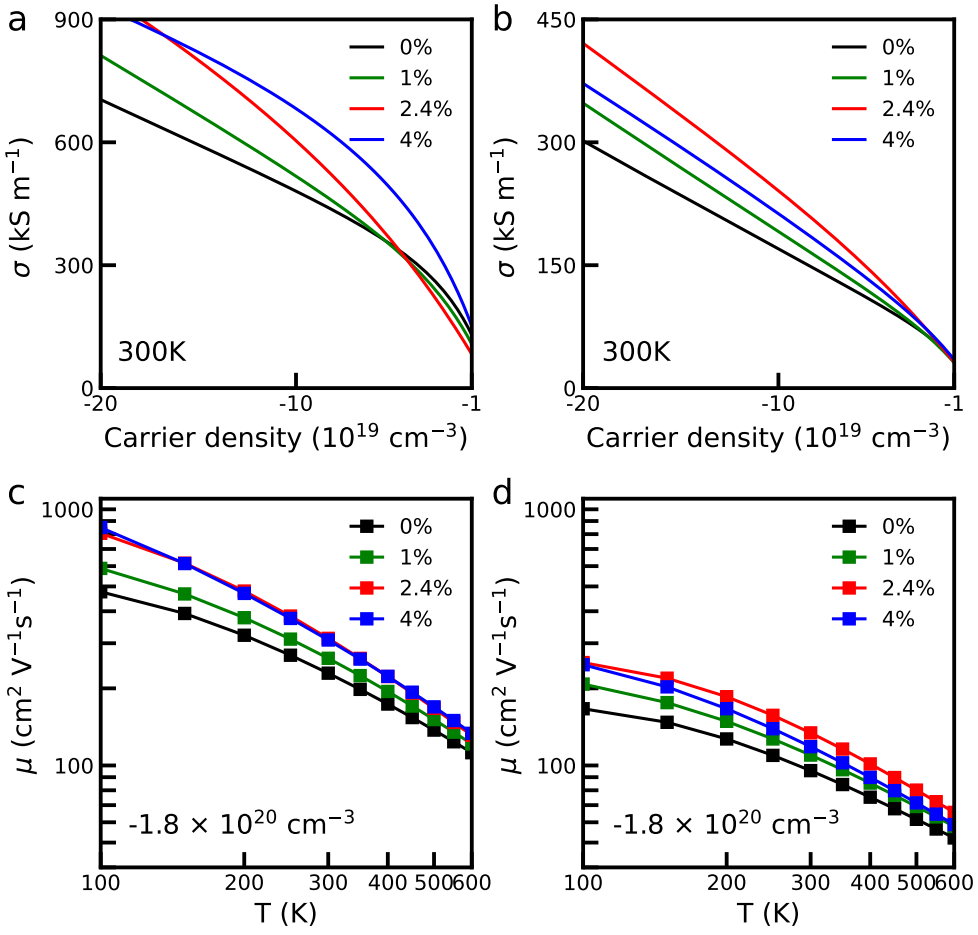

FIG. 3. Electrical conductivity of Mg_2Si under different uniform triaxial tensile strains at 300 K calculated without (**a**) and with (**b**) long-range interaction. Carrier mobility of Mg_2Si (at -1.8 × 10^{20} cm^{-3}) under different tensile strains from 100 K to 600 K calculated without (**c**) and with (**d**) long-range interaction. Electron carrier densities are denoted by negative values.

It is seen that the carrier mobilities of strained Mg_2Si calculated without long-range interaction are much larger than those calculated with long-range interaction, consistent with the results of unstrained Mg_2Si. When the long-range interaction is not considered, the carrier mobilities of Mg_2Si under 2.4% and 4% tensile strains are comparable. If the long-range interaction is considered, carrier mobility under a 2.4% tensile strain becomes the largest. Therefore, the electrical conductivities of Mg_2Si at different band structure configurations are susceptible to the long-range interaction, which is critical to properly studying the effect of band convergence on the electrical transport property.

To better understand the effect of long-range interaction, we further study the electron-phonon scattering mechanism in Mg_2Si. Panels **a** and **b** of Fig. 4 show the electronic scattering rates of Mg_2Si under 2.4% and 4% tensile strains without considering the long-range interaction. The total scattering rate near the CBM under a 2.4% tensile strain is significantly larger than that under a 4% tensile strain, which results in shorter electronic relaxation time and is consistent with the lower electrical conductivity observed under a 2.4% tensile strain (see Fig. 3**a**). Fig. 4**c** and **d** show the electronic scattering rates of Mg_2Si under 2.4% and 4% tensile strains calculated with long-range interaction. It is seen that the total electronic scattering rates of Mg_2Si become much larger than those calculated without long-range interaction. Correspondingly, the electronic relaxation time is much shorter when the long-range interaction is considered, resulting in the suppressed electrical conductivity and carrier mobility (see Fig. 1 and Fig. 3). With long-range interaction, the difference of the total electronic scattering rate between 2.4% and 4% tensile strains near the CBM also becomes smaller.

Figs. S5 and S6 of the Supporting Information show the mode-resolved electronic scattering rates of unstrained Mg_2Si calculated without and with long-range interaction, respectively. The indexes of phonon modes are sorted according to their frequencies from low to high. It is seen from Figs. S5 and S6 that electronic scatterings by #3 and #9 phonon modes are much stronger than that by other phonon modes; therefore, we focus on these two phonon modes. When long-range interaction is not considered, electronic scatterings by #3 and #9 phonon modes are comparable under a 2.4% tensile strain, and electronic scattering by #9 phonon mode is suppressed under a 4% tensile strain (see Fig. 4**a** and **b**). When the long-range interaction is taken into account, electronic scattering by #9 phonon mode becomes significantly stronger than that by #3 phonon mode under different tensile strains,

indicating that the electron-phonon scattering of Mg_2Si is dominated by the highest phonon mode at different band structure configurations. We see from the results that the presence of long-range interaction is critical for a correct understanding of the electron-phonon scattering mechanism in Mg_2Si.

The role of long-range interaction on the electrical conductivity, carrier mobility, and electronic scattering rate of thermoelectric Mg_2Si is studied. With long-range interaction, the electronic scattering rate is found to be significantly increased, resulting in a better

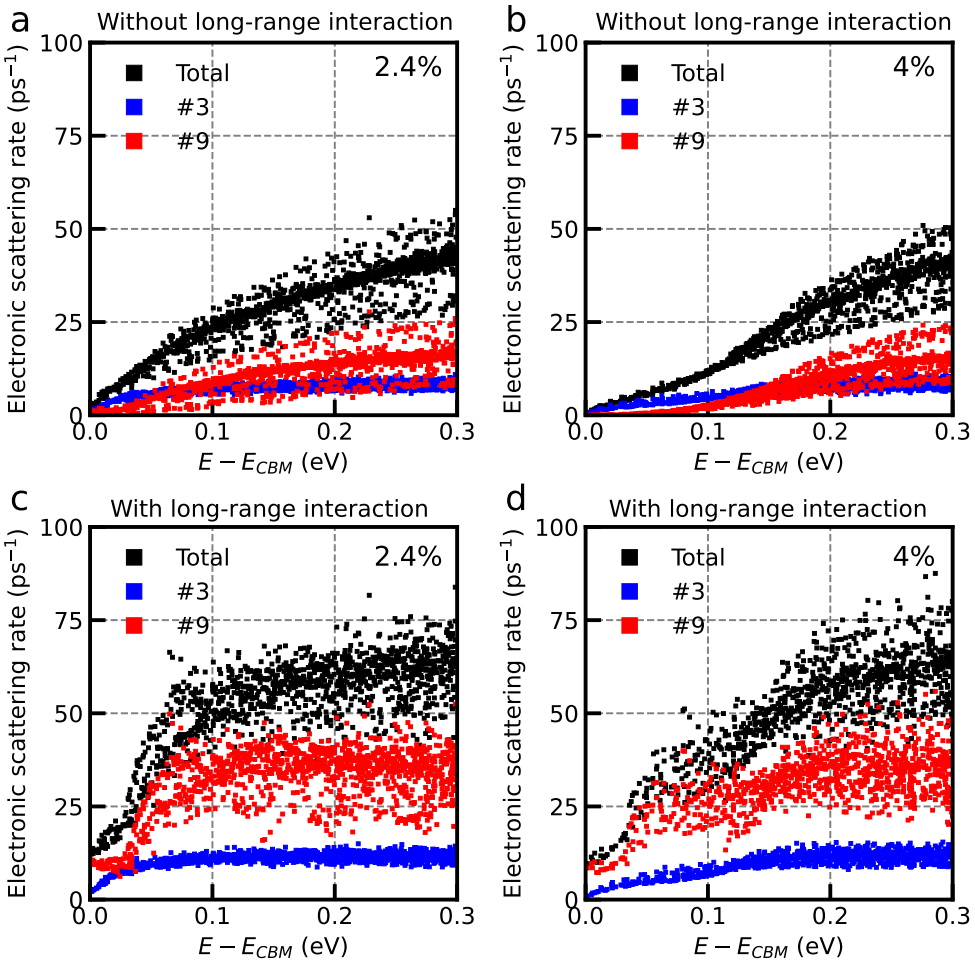

FIG. 4. Panels **a** and **b**: electronic scattering rates of Mg_2Si (at 300 K) under 2.4% and 4% tensile strains calculated without considering long-range interaction. Panels **c** and **d**: electronic scattering rates of Mg_2Si (at 300 K) under 2.4% and 4% tensile strains calculated with long-range interaction. #3 and #9 represent the third and the ninth phonon modes, respectively, sorted according to the frequencies from low to high.

agreement of the theoretical electrical conductivity and carrier mobility of Mg_2Si with the experimental data. In contrast, if the long-range interaction is neglected, the theoretical electrical conductivity of Mg_2Si can be about 3-4 times higher than the experimental value. In addition, the long-range interaction plays an important role in the analysis of electrical transport property and electron-phonon scattering mechanism when studying the effect of band convergence on thermoelectric materials. On the one hand, we find that if long-range interaction is considered, the highest electrical conductivity of strained Mg_2Si is achieved when the conduction bands converge at X point; if it is not considered, the highest electrical conductivity exists at a non-converged band structure configuration. On the other hand, the contribution of the highest phonon mode to electron-phonon scattering is underestimated in Mg_2Si if the long-range interaction is neglected. The presence of long-range interaction is fundamental to understanding the electron-phonon interaction in thermoelectric Mg_2Si.

ACKNOWLEDGMENTS

This work is supported by the Zhejiang Provincial Natural Science Foundation (LR19A040001), the Research Grants Council of Hong Kong (17201019 and 17306721), and the National Natural Science Foundation of China (11874313). The authors are grateful for the research computing facilities offered by ITS, HKU.

The data that support the findings of this study are available from the corresponding author upon reasonable request.

REFERENCES

[1]J. He, Y. Xia, S. S. Naghavi, V. Ozoliņš, and C. Wolverton, "Designing chemical analogs to PbTe with intrinsic high band degeneracy and low lattice thermal conductivity," Nature Communications **10**, 719 (2019).

[2]J. Park, Y. Xia, A. M. Ganose, A. Jain, and V. Ozoliņš, "High Thermoelectric Performance and Defect Energetics of Multipocketed Full Heusler Compounds," Phys. Rev. Applied **14**, 024064 (2020).

[3]J. Park, Y. Xia, V. Ozoliņš, and A. Jain, "Optimal band structure for thermoelectrics with realistic scattering and bands," *npj* Computational Materials **7**, 43 (2021).

[4]C. Xia, J. Cui, and Y. Chen, "Optimization of the Intrinsic Electrical and Thermal Transport Properties of $Sb_2Si_2Te_6$ via Tensile Strain: A First-Principles Study," ACS Applied Energy Materials **4**, 12285–12289 (2021).

[5]S. Huang, Z. Wang, R. Xiong, H. Yu, and J. Shi, "Significant enhancement in thermoelectric performance of Mg_3Sb_2 from bulk to two-dimensional mono layer," Nano Energy **62**, 212–219 (2019).

[6]S. Poncé, E. R. Margine, and F. Giustino, "Towards predictive many-body calculations of phonon-limited carrier mobilities in semiconductors," Phys. Rev. B **97**, 121201 (2018).

[7]Y. Xia, J. Park, V. Ozoliņš, and C. Wolverton, "Leveraging electron-phonon interaction to enhance the thermoelectric power factor in graphene-like semimetals," Phys. Rev. B **100**, 201401 (2019).

[8]J. Zhou, H. Zhu, T.-H. Liu, Q. Song, R. He, J. Mao, Z. Liu, W. Ren, B. Liao, D. J. Singh, Z. Ren, and G. Chen, "Large thermoelectric power factor from crystal symmetry-protected non-bonding orbital in half-Heuslers," Nature Communications **9**, 1721 (2018).

[9]Y. Wu, B. Hou, C. Ma, J. Cao, Y. Chen, Z. Lu, H. Mei, H. Shao, Y. Xu, H. Zhu, Z. Fang, R. Zhang, and H. Zhang, "Thermoelectric performance of 2D materials: the band-convergence strategy and strong intervalley scatterings," Mater. Horiz. **8**, 1253–1263 (2021).

[10]F. Giustino, M. L. Cohen, and S. G. Louie, "Electron-phonon interaction using Wannier functions," Phys. Rev. B **76**, 165108 (2007).

[11]F. Giustino, "Electron-phonon interactions from first principles," Rev. Mod. Phys. **89**, 015003 (2017).

[12]O. D. Restrepo, K. Varga, and S. T. Pantelides, "First-principles calculations of electron mobilities in silicon: Phonon and Coulomb scattering," Applied Physics Letters **94**, 212103 (2009).

[13]C.-H. Park, N. Bonini, T. Sohier, G. Samsonidze, B. Kozinsky, M. Calandra, F. Mauri, and N. Marzari, "Electron–phonon interactions and the intrinsic electrical resistivity of graphene," Nano Letters **14**, 1113–1119 (2014).

[14]C. Verdi and F. Giustino, "Fröhlich electron-phonon vertex from first principles," Phys. Rev. Lett. **115**, 176401 (2015).

[15]Q. Song, T.-H. Liu, J. Zhou, Z. Ding, and G. Chen, "Ab initio study of electron mean free paths and thermoelectric properties of lead telluride," Materials Today Physics **2**, 69–77

(2017).

[16]J.-J. Zhou and M. Bernardi, "Ab initio electron mobility and polar phonon scattering in GaAs," Phys. Rev. B **94**, 201201 (2016).

[17]T.-H. Liu, J. Zhou, B. Liao, D. J. Singh, and G. Chen, "First-principles mode-by-mode analysis for electron-phonon scattering channels and mean free path spectra in GaAs," Phys. Rev. B **95**, 075206 (2017).

[18]F. Meng, J. Ma, J. He, and W. Li, "Phonon-limited carrier mobility and temperature-dependent scattering mechanism of $3C$-SiC from first principles," Phys. Rev. B **99**, 045201 (2019).

[19]J.-J. Zhou, O. Hellman, and M. Bernardi, "Electron-Phonon Scattering in the Presence of Soft Modes and Electron Mobility in $SrTiO_3$ Perovskite from First Principles," Phys. Rev. Lett. **121**, 226603 (2018).

[20]V. A. Jhalani, J.-J. Zhou, J. Park, C. E. Dreyer, and M. Bernardi, "Piezoelectric Electron-Phonon Interaction from Ab Initio Dynamical Quadrupoles: Impact on Charge Transport in Wurtzite GaN," Phys. Rev. Lett. **125**, 136602 (2020).

[21]J. Cao, J. D. Querales-Flores, A. R. Murphy, S. Fahy, and I. Savić, "Dominant electron-phonon scattering mechanisms in n-type PbTe from first principles," Phys. Rev. B **98**, 205202 (2018).

[22]R. D'Souza, J. Cao, J. D. Querales-Flores, S. Fahy, and I. Savić, "Electron-phonon scattering and thermoelectric transport in p-type PbTe from first principles," Phys. Rev. B **102**, 115204 (2020).

[23]J. Ding, C. Liu, L. Xi, J. Xi, and J. Yang, "Thermoelectric transport properties in chalcogenides ZnX (X=S, Se): From the role of electron-phonon couplings," Journal of Materiomics **7**, 310–319 (2021).

[24]J. Ma, Y. Chen, and W. Li, "Intrinsic phonon-limited charge carrier mobilities in thermoelectric SnSe," Phys. Rev. B **97**, 205207 (2018).

[25]Y. Pei, X. Shi, A. LaLonde, H. Wang, L. Chen, and G. J. Snyder, "Convergence of electronic bands for high performance bulk thermoelectrics," Nature **473**, 66–69 (2011).

[26]W. Liu, X. Tan, K. Yin, H. Liu, X. Tang, J. Shi, Q. Zhang, and C. Uher, "Convergence of Conduction Bands as a Means of Enhancing Thermoelectric Performance of n-Type $Mg_2Si_{1-x}Sn_x$ Solid Solutions," Phys. Rev. Lett. **108**, 166601 (2012).

[27]Y. Tang, Z. M. Gibbs, L. A. Agapito, G. Li, H.-S. Kim, M. B. Nardelli, S. Curtarolo, and

G. J. Snyder, "Convergence of multi-valley bands as the electronic origin of high thermoelectric performance in $CoSb_3$ skutterudites," Nature Materials **14**, 1223–1228 (2015).

[28]A. Banik, U. S. Shenoy, S. Anand, U. V. Waghmare, and K. Biswas, "Mg Alloying in SnTe Facilitates Valence Band Convergence and Optimizes Thermoelectric Properties," Chemistry of Materials **27**, 581–587 (2015).

[29]K. Imasato, S. D. Kang, S. Ohno, and G. J. Snyder, "Band engineering in Mg_3Sb_2 by alloying with Mg_3Bi_2 for enhanced thermoelectric performance," Mater. Horiz. **5**, 59–64 (2018).

[30]C. Xia, J. Cui, and Y. Chen, "Effect of group-3 elements doping on promotion of in-plane seebeck coefficient of n-type Mg_3Sb_2," Journal of Materiomics **6**, 274–279 (2020).

[31]C. Xia, J. Cui, and Y. Chen, "Modulation of Band Alignment and Electron–Phonon Scattering in Mg_3Sb_2 via Pressure," ACS Applied Electronic Materials **2**, 2745–2749 (2020).

[32]J. Zhang, R. Liu, N. Cheng, Y. Zhang, J. Yang, C. Uher, X. Shi, L. Chen, and W. Zhang, "High-performance pseudocubic thermoelectric materials from non-cubic chalcopyrite compounds," Advanced Materials **26**, 3848–3853 (2014).

[33]W. G. Zeier, H. Zhu, Z. M. Gibbs, G. Ceder, W. Tremel, and G. J. Snyder, "Band convergence in the non-cubic chalcopyrite compounds Cu_2MGeSe_4," J. Mater. Chem. C **2**, 10189–10194 (2014).

[34]J. Park, M. Dylla, Y. Xia, M. Wood, G. J. Snyder, and A. Jain, "When band convergence is not beneficial for thermoelectrics," Nature Communications **12**, 3425 (2021).

[35]P. Hohenberg and W. Kohn, "Inhomogeneous Electron Gas," Phys. Rev. **136**, B864–B871 (1964).

[36]W. Kohn and L. J. Sham, "Self-Consistent Equations Including Exchange and Correlation Effects," Phys. Rev. **140**, A1133–A1138 (1965).

[37]P. Giannozzi, S. Baroni, N. Bonini, M. Calandra, R. Car, C. Cavazzoni, D. Ceresoli, G. L. Chiarotti, M. Cococcioni, I. Dabo, A. D. Corso, S. de Gironcoli, S. Fabris, G. Fratesi, R. Gebauer, U. Gerstmann, C. Gougoussis, A. Kokalj, M. Lazzeri, L. Martin-Samos, N. Marzari, F. Mauri, R. Mazzarello, S. Paolini, A. Pasquarello, L. Paulatto, C. Sbraccia, S. Scandolo, G. Sclauzero, A. P. Seitsonen, A. Smogunov, P. Umari, and R. M. Wentzcovitch, "QUANTUM ESPRESSO: a modular and open-source software project for quantum simulations of materials," Journal of Physics: Condensed Matter **21**, 395502 (2009).

[38]P. Giannozzi, O. Andreussi, T. Brumme, O. Bunau, M. B. Nardelli, M. Calandra,

R. Car, C. Cavazzoni, D. Ceresoli, M. Cococcioni, N. Colonna, I. Carnimeo, A. D. Corso, S. de Gironcoli, P. Delugas, R. A. DiStasio, A. Ferretti, A. Floris, G. Fratesi, G. Fugallo, R. Gebauer, U. Gerstmann, F. Giustino, T. Gorni, J. Jia, M. Kawamura, H.-Y. Ko, A. Kokalj, E. Küçükbenli, M. Lazzeri, M. Marsili, N. Marzari, F. Mauri, N. L. Nguyen, H.-V. Nguyen, A. O. de-la Roza, L. Paulatto, S. Poncé, D. Rocca, R. Sabatini, B. Santra, M. Schlipf, A. P. Seitsonen, A. Smogunov, I. Timrov, T. Thonhauser, P. Umari, N. Vast, X. Wu, and S. Baroni, "Advanced capabilities for materials modelling with QUANTUM ESPRESSO," Journal of Physics: Condensed Matter **29**, 465901 (2017).

[39]S. Goedecker, M. Teter, and J. Hutter, "Separable dual-space Gaussian pseudopotentials," Phys. Rev. B **54**, 1703–1710 (1996).

[40]C. Hartwigsen, S. Goedecker, and J. Hutter, "Relativistic separable dual-space Gaussian pseudopotentials from H to Rn," Phys. Rev. B **58**, 3641–3662 (1998).

[41]S. Poncé, E. Margine, C. Verdi, and F. Giustino, "EPW: Electron–phonon coupling, transport and superconducting properties using maximally localized wannier functions," Computer Physics Communications **209**, 116–133 (2016).

[42]G. K. Madsen, J. Carrete, and M. J. Verstraete, "BoltzTraP2, a program for interpolating band structures and calculating semi-classical transport coefficients," Computer Physics Communications **231**, 140–145 (2018).

[43]J. ichi Tani and H. Kido, "Thermoelectric properties of Bi-doped Mg_2Si semiconductors," Physica B: Condensed Matter **364**, 218–224 (2005).

[44]J. ichi Tani and H. Kido, "Thermoelectric properties of Sb-doped Mg_2Si semiconductors," Intermetallics **15**, 1202–1207 (2007).

[45]N. Farahi, M. VanZant, J. Zhao, J. S. Tse, S. Prabhudev, G. A. Botton, J. R. Salvador, F. Borondics, Z. Liu, and H. Kleinke, "Sb- and Bi-doped Mg_2Si: location of the dopants, micro- and nanostructures, electronic structures and thermoelectric properties," Dalton Trans. **43**, 14983–14991 (2014).

[46]G. S. Nolas, D. Wang, and M. Beekman, "Transport properties of polycrystalline $Mg_2Si_{1-y}Sb_y$ ($0 \leq y < 0.4$)," Phys. Rev. B **76**, 235204 (2007).

[47]V. Askarpour and J. Maassen, "Unusual thermoelectric transport anisotropy in quasi-two-dimensional rhombohedral GeTe," Phys. Rev. B **100**, 075201 (2019).

[48]F. Meng, S. Sun, J. Ma, C. Chronister, J. He, and W. Li, "Anisotropic thermoelectric figure-of-merit in Mg_3Sb_2," Materials Today Physics **13**, 100217 (2020).

[49]K. Kutorasiński, J. Tobola, and S. Kaprzyk, "Calculating electron transport coefficients of disordered alloys using the KKR-CPA method and boltzmann approach: Application to $Mg_2Si_{1-x}Sn_x$ thermoelectrics," Phys. Rev. B **87**, 195205 (2013).

[50]N. Hirayama, Y. Imai, and N. Hamada, "Conduction band engineering of Mg_2Si by isotropic strain for enhancement of thermoelectric performance: A first-principles study," Journal of Applied Physics **127**, 205107 (2020).